Greenhouse gas measurement campaign of the Earth Summit Mission-2022: ground-based *in situ* and FTIR observations and contributes to satellite validation in the Qomolangma region

Minqiang Zhou[1,3], Yilong Wang[2,3*], Minzheng Duan[3,4*], Xiangjun Tian[2,3], Jinzhi Ding[2,3], Jianrong Bi[5], Yaoming Ma[2,6], Weiqiang Ma[2,6], Zhenhua Xi[2,6]

[1] *State Key Laboratory of Atmospheric Environment and Extreme Meteorology, Institute of Atmospheric Physics, Chinese Academy of Sciences, Beijing* 100029, *China*

[2] *State Key Laboratory of Tibetan Plateau Earth System, Environment and Resources, Institute of Tibetan Plateau Research, Chinese Academy of Sciences, Beijing 100101, China*

[3] *University of Chinese Academy of Sciences, Beijing 100049, China*

[4] *Key Laboratory for Middle Atmosphere and Global Environment Observation, Institute of Atmospheric Physics, Chinese Academy of Sciences, Beijing* 100029, *China*

[5] *Key Laboratory for Semi-Arid Climate Change of the Ministry of Education, College of Atmospheric Sciences, Lanzhou University, Lanzhou, China*

[6]*National Observation and Research Station for Qomolangma Special Atmospheric Processes and Environmental Changes, Dingri 858200, China*

Corresponding authors: Yilong Wang (wangyilong@itpcas.ac.cn) and Minzheng Duan (dmz@mail.iap.ac.cn)

Abstract

The Qinghai-Tibetan Plateau (QTP) is a key system that impacts the global carbon balance, but greenhouse gases (GHGs) mole fraction measurements in this region are limited due to the tough environment. Supported by the Second Tibetan Plateau Scientific Expedition Program, we carried out an integrated GHG measurement campaign in May 2022 as part of the Earth Summit Mission-2022 at the Qomolangma station for atmospheric and environmental observation and research (QOMS; 28.362°N, 86.949°E, 4276 m a.s.l.). In this study, the first GHG column-averaged mole fraction measurements (Xgas) at QOMS are presented, including XCO_2, XCH_4, XCO, and XN_2O, derived from a ground-based Fourier-transform infrared spectrometer (FTIR; Bruker EM27/SUN). We then compare them to surface *in situ* and satellite (TROPOMI and OCO-2) measurements. The

mean FTIR XCO_2 and XCH_4 are 7.8 ppm and 97 ppb less than those near the surface, respectively. The difference between OCO-2 land nadir and EM27/SUN XCO_2 measurements is 0.21±0.98 ppm, which is consistent with OCO-2 retrieval uncertainty. However, a relatively large bias (1.21±1.29 ppm) is found for OCO-2 glint XCO_2 measurements, which is related to the surface albedos and surface altitudes. The EM27/SUN measurements indicate that the uncertainty of OCO-2 satellite XCO_2 measurements is relatively large in the QTP mountain region and its quality needs to be further assessed. The difference between FTIR and TROPOMI XCO measurements is -5.06±5.36 (1σ) ppb (-4.7±5.1%) within the satellite retrieval uncertainty. The XCO measurements at QOMS show the local airmass is largely influenced by atmospheric transport from southern Asia, and it is important to carry out long-term measurements to quantify the contribution of the cross-regional transport in this region.

Keywords: Qomolangma, greenhouse gas, EM27/SUN, OCO-2, TROPOMI

1 Introduction

The Qinghai-Tibetan Plateau (QTP) plays an important role in regional and global climate systems (Ge et al. 2017; Tada et al. 2016; Zhang et al. 2021). The high mountains in the QTP, including the Earth's highest summit (Mt. Qomolangma; 8848.86 m a.s.l.), strongly affect the atmospheric thermodynamic and dynamic conditions. On the other hand, environmental changes, including human activities, atmospheric warming, and cryosphere thaw, can in turn make significant impacts on the hydrology, ecosystems, and biogeochemistry in the QTP (Rui et al. 2011; Wu et al. 2021; Zhang et al. 2015). The QTP has abundant original forest and soil resources, and serves as a huge carbon storage (Ding et al. 2016; Wang et al. 2020; Jia et al. 2021). A small change in carbon storage of the QTP could make an impact on the global carbon balance. However, there is still a large uncertainty about the terrestrial ecosystem carbon sink in the QTP (Wang et al. 2021; Piao et al. 2022). The uncertainties associated with eddy covariance data processing may lead to an overestimation of the carbon sink (Wang et al. 2022). Using a 'top-down' approach can help us to estimate the carbon sink in the QTP (Jiang et al. 2016). However, limited greenhouse gases (GHGs) measurements are currently available in this region because of the tough environment (Guo et al. 2020; Liu et al. 2021; Zhou et al. 2023).

To better understand the level and temporal variation of atmospheric GHGs mole fraction over the QTP, we carried out an integrated GHGs measurement campaign at the Qomolangma station for atmospheric and environmental observation and research, Chinese Academy of Sciences (QOMS) in May 2022 as part of the Second Tibetan Plateau Scientific Expedition Program (Earth Summit Mission-2022). During this campaign, a compact Fourier-transform infrared spectrometer (FTIR), Bruker EM27/SUN, was applied to retrieve the column-averaged dry air mole fraction of CO_2, CH_4, CO, and N_2O (XCO_2, XCH_4, XCO, and XN_2O) at QOMS between 5 and 24 May 2022. The FTIR measures the GHG columns, which are less affected by the local meteorological parameters, such as the boundary layer height and wind turbulence (Wunch et al. 2011; Zhou et al. 2018). The ground-based FTIR GHGs measurement is widely used to validate satellite observation because of its high precision and similar measurement technique to the satellite (Zhou et al. 2016; Wunch et al. 2017; Sha et al. 2021). In addition, a gas analyzer (ABB Ultra-Portable Greenhouse Gas Analyzer; GLA132), using a off-axis integrated cavity output spectroscopy (OA-ICOS) technique, was applied to measure the CO_2 and CH_4 mole fractions near the surface. In the following sections, we will give an introduction to the observation site, and present the XCO_2, XCH_4, XCO, and XN_2O derived from the EM27/SUN FTIR spectra at QOMS. The results from the *in situ* and ground-based FTIR measurements are shown in Section 3. In Section 4, the *in situ* surface measurements are compared to the FTIR column measurements. Moreover, the FTIR measurements are then compared to independent satellite observations. Finally, the conclusions are drawn in Section 5.

2 Observation site and data

2.1 The QOMS site

The QOMS (latitude 28.362°N; longitude 86.949°E; with an elevation of 4276 m a.s.l.) is situated approximately 30 km away from the Everest Base Camp and around 650 km from Lhasa (Figure 1). The station is located about 3 km to the south of the local village, in an area with minimal human influence. The surface of the station is flat, and it is mainly covered by sand and gravel with sparse vegetation. More information about the QOMS refers to Ma et al. (2023).

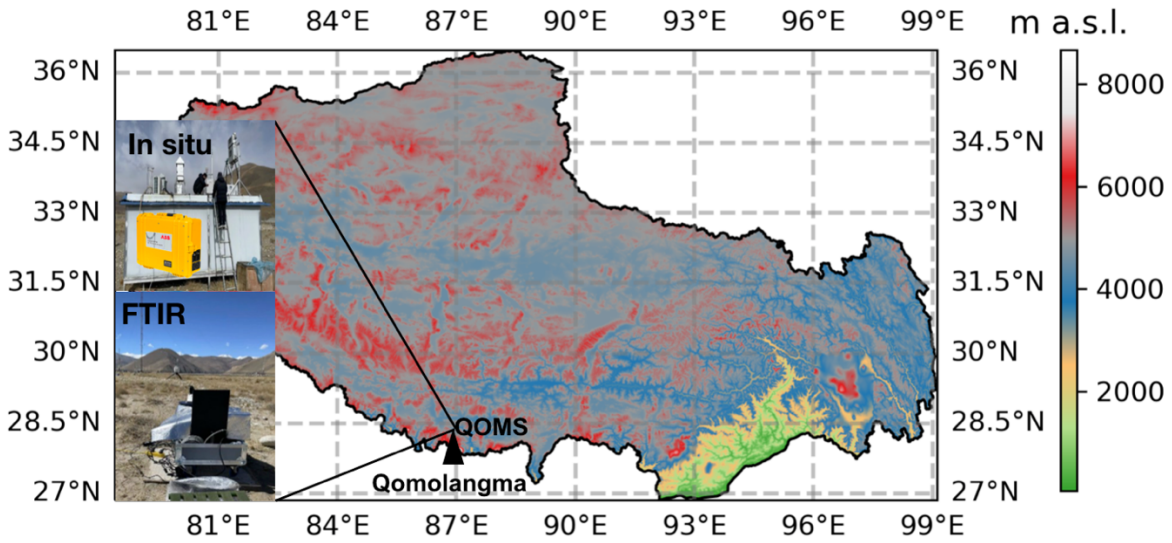

Figure 1. The integrated GHGs measurement campaign carried out at the Qomolangma station for atmospheric and environmental observation and research station (QOMS) in May 2022 including both the FTIR remote sensing and surface *in situ* measurements.

2.2 Ground-based FTIR

A Bruker EM27/SUN FTIR was operated at QOMS between 5 and 24 May. The measurement settings of the EM27/SUN follow the guidance of the COllaborative Carbon Column Observing Network (COCCON), which records the direct solar absorption spectra between 4000 and 12000 cm^{-1} with a spectral resolution of 0.5 cm^{-1} using two InGaAs detectors (Frey et al., 2019). The advanced retrieval algorithm GGG2020 is applied to retrieve the O_2 and GHGs (CO_2, CH_4, CO, and N_2O) total columns, and then Xgas is calculated as 0.2095 (TC_{GHG}/TC_{o_2}). Using the ratio between target species and O_2 can reduce the same uncertainty from the instrumental and atmospheric parameters (Yang et al. 2002). GGG2020 is commonly used in the ground-based GHG remote sensing community, and it includes: 1) the conversion from interferogram to spectrum with the DC correction (Keppel-Aleks et al. 2012); 2) a non-linear least squares fitting code (GFIT); 3) a post-correction procedure to reduce the retrieval uncertainty resulting from spectroscopy and observation geometry (Laughner et al. 2023). We have observed the EM27/SUN instrument line shape (ILS) parameters before and after the campaign in the lab. Both the Modulation efficiency and phase error keep almost unchanged before and after the campaign, reflecting that the instrument was well protected during the long-distance transportation. Table A1 in appendix I shows the systematic and random uncertainties of CO_2, CH_4, CO and N_2O column

retrievals are 2.0%/0.2%, 2.0%/0.2%, 2.0%/0.9%, and 2.0%/1.2%, respectively. The systematic uncertainty is dominated by the spectroscopy. To further reduce the systematic uncertainty of the EM27/SUN retrievals, the EM27/SUN instrument was operated together with the TCCON site at Xianghe (Yang et al. 2020) for three weeks in July-August 2022 after the campaign. Based on the co-located measurements of EM27/SUN and TCCON, the scaling factors of 1.001, 0.995, 0.970, and 1.004 have been derived and applied to correct the systematic uncertainties of the EM27/SUN XCO_2, XCH_4, XCO, and XN_2O retrievals, respectively.

2.3 In situ

The near-surface CO_2 and CH_4 mole fractions were observed by the ABB GLA132 gas analyzer at QOMS continuously between 13 and 24 May 2022 (Figure 1). To ensure the accuracy of the GHG *in situ* measurements, we calibrated the gas analyzer using the standard gas once per day. The precisions of the *in situ* measurements (1 second) are within 0.3 ppm and 2.0 ppb for CO_2 and CH_4, respectively (https://www.envicontrol.com/storage/app/media/uploaded-files/UGGA%20LGR%20GLA132-GGA.pdf). Note that the drifts of CO_2 and CH_4 within 24 hours of the analyzer are within their measurement uncertainties.

2.4 Satellite

We use the Orbiting Carbon Observatory-2 (OCO-2) satellite level 2 bias-corrected XCO_2 retrospective processing v11.2r (Kiel et al. 2019). The OCO-2 XCO_2 is retrieved using the ACOS algorithm by the CO_2 absorption lines around 1.61 and 2.06 μm, together with the information about surface pressure, cloud and aerosol scattering constrained by the O_2-A band around 0.76μm (O'dell et al. 2018). For more details about the OCO-2 XCO_2 data, we refer to the https://docserver.gesdisc.eosdis.nasa.gov/public/project/OCO/OCO_L2_ATBD.pdf. The OCO-2 XCO_2 uncertainty has been accessed by comparing to the Total Carbon Column Observing Network (TCCON), and the absolute median difference across TCCON sites over the globe is found to be less than 0.4 ppm and the root mean square of the differences is less than 1.5 ppm (Wunch et al. 2017). The footprint size of each OCO-2 pixel is 2.25×1.29 km^2. However, the width of the swath is only about 16 km, leading to a very small spatial coverage. During the campaign, there were 2 days when the orbit of OCO-2 overpassed within 500 km around QOMS. These OCO-2 satellite measurements are compared to EM27/SUN FTIR measurements to assess their quality at QOMS.

Regarding CH_4 and CO, we use the ESA operational offline level 2 products from the Sentinel-5 Precursor (S5-P) TROPOspheric Monitoring Instrument (TROPOMI). Unfortunately, there is almost no TROPOMI CH_4 retrieval at QOMS, mainly due to the complex orography and high cloud coverage in this region (Lorente et al. 2021). Therefore, in this study, we only look at the TROPOMI XCO data. The TROPOMI XCO retrievals are derived from the reflected solar radiation in 2.3 μm band and the stripes of erroneous XCO retrievals are corrected by the fixed masked de-striping method (Landgraf et al. 2016; Borsdorff et al. 2019). The spatial resolution of TROPOMI measurements is 7.0×5.5 km^2. Thanks to the large swath of about 2600 km, TROPOMI provides XCO measurements in this region around 15:30 China Standard Time (CST) every day. According to the validation study made by Martínez-Alonso et al. (2022), the mean difference between TROPOMI XCO data and AirCore measurements is 2.02±11.13 (1σ) %.

3 Results

3.1 Ground-based FTIR column measurements

The time series together of *a priori* and retrieved XCO_2, XCH_4, XCO, and XN_2O measurements from the EM27/SUN FTIR at QOMS between 5 and 24 May are shown in Figure 2. The *a priori* columns of FTIR retrievals are derived from the global atmospheric chemistry model (GEOS-FPIT), which provides 6-hourly simulations with a spatial resolution of about 50 km. For more information about the GGG2020 *a priori* profiles, please refer to Laughner et al. (2023). Keep in mind that the FTIR provides the measurements only in the daytime and under a clear sky condition.

The mean and standard deviation (std) of XCO_2, XCH_4, XCO, and XN_2O are 418.4±0.6 ppm, 1888.3±8.0 ppb, 106.2±8.3 ppb, and 321.6±3.2 ppb, respectively. The EM27/SUN retrieved columns are larger than the *a priori* columns for all these four species, indicating that the TCCON prior is systematically underestimated in this region. In addition, the amplitudes of the variations of XCO_2 and XCH_4 derived from the EM27/SUN measurements are larger than the model simulations. Moreover, the day-to-day variations of these species are not well captured by the GEOS-PFIT model, for example, the maximum XCO value observed by the FTIR measurements on 16 May is not well-simulated in the model. The mean of XCO_2, XCH_4, and XCO observed at QOMS are also compared to seven TCCON sites (Hase et al. 2023; Té et al. 2022; Warneke et al. 2022; Wennberg et al. 2022a,b; Zhou et al. 2022; García et al., 2022) in the northern hemisphere

during the same time period (Table 1). The mean XCO_2 at QOMS is lowest among these sites, which is about 1.5-3.5 ppm less than urban sites, and about 0.5-1.5 ppm less than suburban sites and the mountain site (Izaña). The XCH_4 and XCO observed at QOMS are less than those at Xianghe and Caltech, but larger than other TCCON sites.

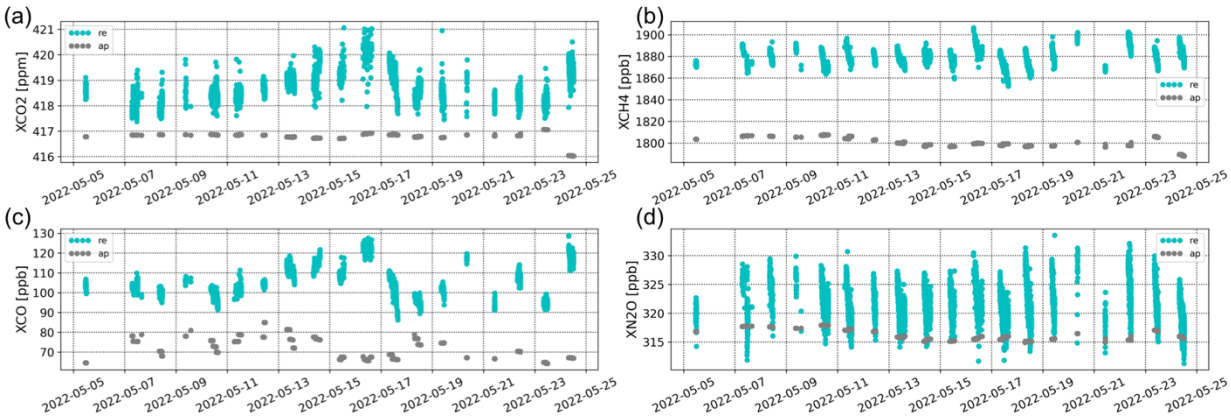

Figure 2. The time series of *a priori* (grey dots) and retrieved (cyan dots) XCO_2, XCH_4, XCO, and XN_2O measurements from the EM27/SUN FTIR between 5 and 24 May 2022 at QOMS.

Table 1. The mean and std of the XCO_2, XCH_4, XCO measurements at six TCCON sites in the northern hemisphere, together with our EM27/SUN measurements at QOMS. N is the number of measurements at each site between 5 and 24 May 2022.

Type	Site	Geolocation	XCO_2 (ppm)	XCH_4 (ppb)	XCO (ppb)	N
Urban	Paris	48.84°N;2.35°E;60 m	420.1±0.9	1870.4±4.2	97.9±7.2	685
	Xianghe	39.8°N;116.96°E;36 m	419.9±0.8	1906.7±12.1	134.4±15.3	268
	Caltech	34.13°N;118.12°W;230m	421.9±0.9	1899.2±6.8	117.6±6.4	1956
Suburb	Karlsruhe	49.1°N;8.439°E;116 m	418.9±0.8	1876.3±9.2	99.2±3.9	533
	Orleans	47.97°N;2.113°E;130m	418.9±0.8	1875.9±7.5	96.2±5.9	1641
	Lamont	36.6°N;97.486°W;320 m	419.9±0.7	1885.6±6.1	105.1±7.8	838
Mountain	Izaña	28.3°N;16.499°E;2367 m	419.8±0.4	1873.5±4.6	81.7±2.7	819
QTP	QOMS	28.3°N; 86.9°E; 4276 m	418.4±0.6	1888.3±8.0	106.2±8.3	5925

Figure 3 shows the covariance matrix among these four species observed by the EM27/SUN measurements. The good correlations are found between XCO_2 and XCO (R=0.79;

p_value<0.001), XCH_4 and XCO (R=0.63; p_value<0.01), XCH_4 and XN_2O (R=0.77; p_value<0.001). However, the correlations are relatively weak between XCO_2 and XCH_4 (R=0.16; p_value=0.50), XCO_2 and XN_2O (R=-0.20; p_value=0.41), XCO and XN_2O (R=0.19; p_value=0.43). The good correlation between XCH_4 and XN_2O is probably due to their similar physical and chemical process in the stratosphere (Wang et al. 2014; Ji et al. 2020).

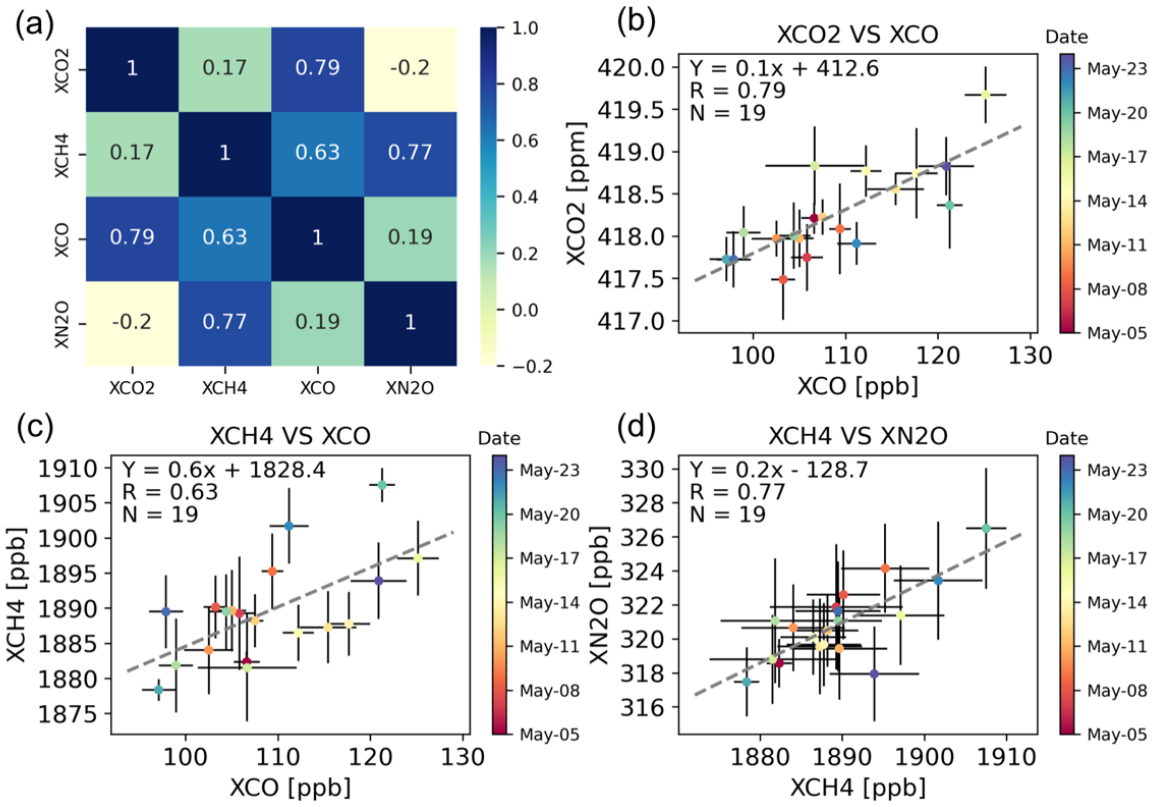

Figure 3. The correlation matrix among XCO_2, XCH_4, XCO and XN_2O observed by the EM27/SUN measurements between 5 and 24 May 2022 at QOMS (a), together with the scatter plots between XCO_2 and XCO daily means (b), between XCH_4 and XCO daily means (c), and XCH_4 and XN_2O daily means (d). In each scatter plot, the error bar denotes the daily std, the dashed line is the linear regression, R is the Pearson correlation coefficient, and N is the number of the co-located measurements. The dot is colored by the measurement date.

The EM27/SUN measurements indicate that XCO is a good tracer for both XCO_2 and XCH_4 at QOMS, while the R between XCO_2 and CH_4 is only 0.17. To better understand this, we separate the time period into 3 weeks (Table 2). The R values are relatively low in the first week, especially between XCO_2 and XCH_4. The day-to-day variations of these species are pretty low in the first week (Figure 2). In the second week, large enhancements of the three species on 16 May

206 are observed simultaneously, resulting in large R values. In the third week, strong vibrations in
207 XCO_2, XCH_4, and XCO are observed, but unlike a single large enhancement in the second week,
208 the enhancements in this week are discontinuous. The R values in the third week are larger than
209 those in the first week, but less than those in the second week. Based on the three weeks, we
210 understand that a good correlation (R=0.83) between XCO_2 and XCH_4 can be also observed when
211 a large continuous enhancement occurs. However, the correlation between XCO_2 and XCH_4
212 becomes low and even negative (R=-0.26), when the variations of XCO_2 and XCH_4 are low.

213

214 **Table 2.** The correlations among XCO_2, XCH_4, and XCO in the first week (5-11 May), second
215 week (12-18 May), and third week (19-24 May).

R	XCO_2 and XCH_4	XCO_2 and XCO	XCH_4 and XCO
Week 1 (5-11 May)	-0.26	0.60	0.46
Week 2 (12-18 May)	0.83	0.91	0.84
Week 3 (19-24 May)	0.40	0.89	0.79

216

217 ### *3.2 In situ CO_2 and CH_4* measurements near the surface

218 The time series of CO_2 and CH_4 observed by the gas analyzer at QOMS near the surface
219 between 13 and 24 May, together with their diurnal variations, are shown in Figure 4. The mean
220 and std of CO_2 and CH_4 are 424.2±2.1 ppm and 1985.2±19.7 ppb, respectively. A good correlation
221 between CO_2 and CH_4 is observed, with a Pearson correlation coefficient (R) of 0.82. Similar to
222 the FTIR XCO_2 and XCH_4, the surface CO_2 and CH_4 mole fractions are the highest on 16 May.
223 The mean CO_2 mole fraction in the daytime is about 0.9 ppm higher than that during the night.
224 Contrary to CO_2, we observe the minimum CH_4 value at around 13:00, which is about 12 ppb less
225 than that at midnight.

226

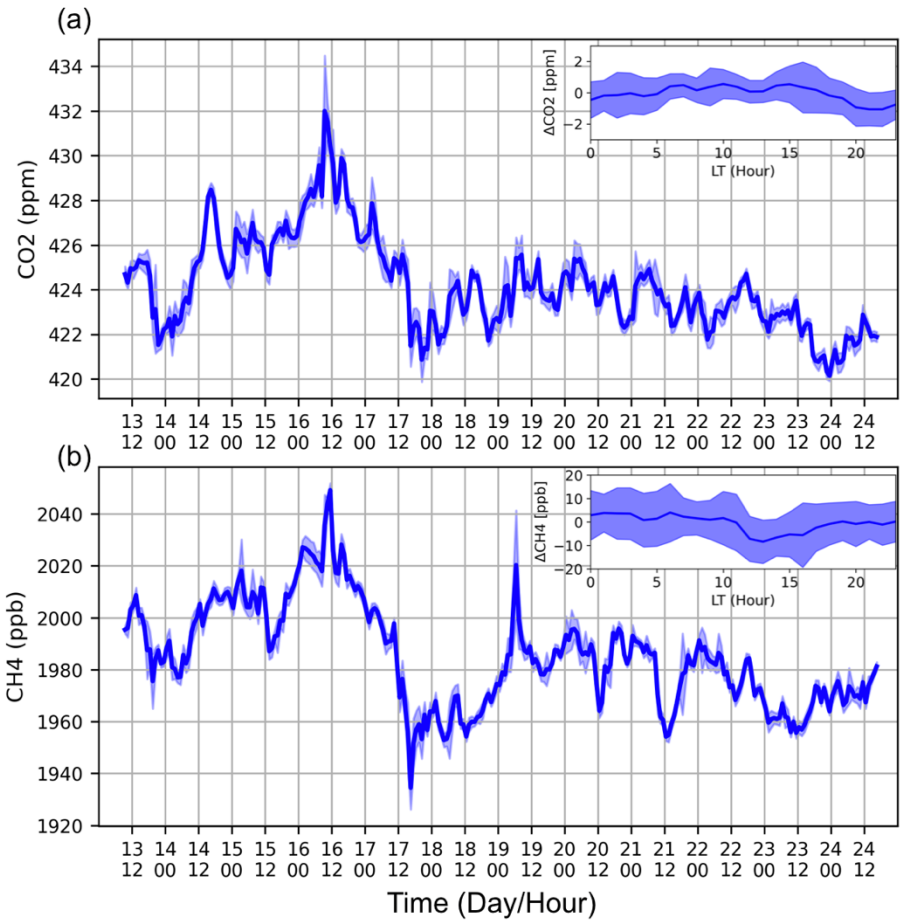

Figure 4. The time series of hourly mean and std of CO_2 (a) and CH_4 (b) mole fraction observed by the gas analyzer at QOMS near the surface. The small panel in the right-upper corner shows the daily variation of CO_2 and CH_4, and the Δgas is derived from the measurements by subtracting the daily median.

4 Inter-comparisons and discussions

4.1 Comparison between FTIR column and surface *in situ* measurements

The FTIR observes the CO_2 and CH_4 columns, while the *in situ* provides the surface mole fractions. Do the variations of XCO_2 and XCH_4 differ from the surface measurements? Here, CO_2 and CH_4 surface mole fractions are compared with the FTIR XCO_2 and XCH_4 measurements (Figure 7). To select the co-located data pair, we use the co-existed FTIR and surface hourly means. The mean CO_2 surface mole fraction is 7.8 ppm larger than the XCO_2, and the amplitude of the variation of CO_2 surface variation during this period is 4.8 times larger than the amplitude of the variation of XCO_2. According to the GEOS-PFIT model, CO_2 mole fraction decreases with altitude, especially above the tropopause height (Laughner et al. 2023). A good correlation between the

surface CO_2 and XCO_2 is found, with an R of 0.74 (p_value<0.001). The CO_2 enhancement on 16 May was observed both near the surface and in the column. We also notice that relatively high XCO_2 was observed on 24 May but with low CO_2 mole fractions at the surface. It is indicated that CO_2 enhancement occurs at high altitudes but not at the surface.

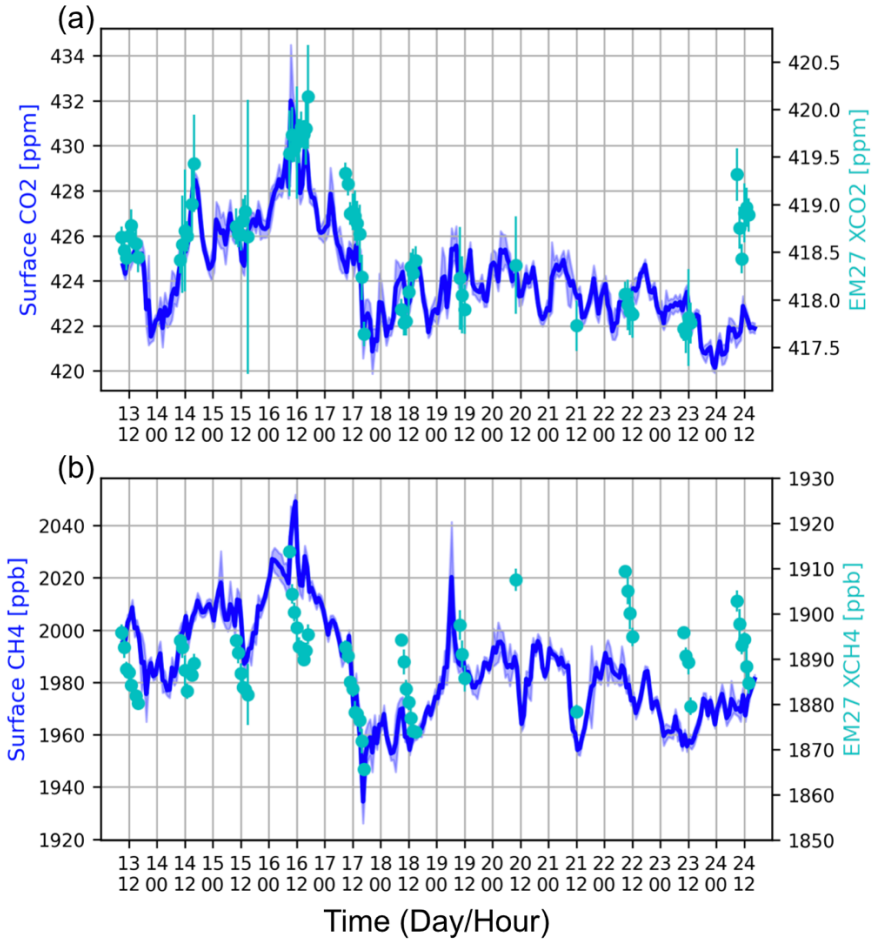

Figure 5. Similar to Figure 4, but adding the EM27/SUN FTIR XCO_2 and XCH_4 hourly means and stds (right y-axis) between 13 and 24 May 2022.

Similar to CO_2, the mean CH_4 surface mole fraction is 97 ppb larger than the XCH_4, and the amplitude of the variation of CH_4 near the surface during this period is 2.9 times larger than the amplitude of the variation of XCH_4. The CH_4 mole fractions in the stratosphere are much lower than those in the troposphere due to the chemical reaction and atmospheric dynamic transport (Sepúlveda et al. 2014; Wang et al. 2014). The correlation between the surface CH_4 and XCH_4 is relatively weak as compared to that between CO_2 and XCO_2 but still statistically significant (R=0.41; p_value<0.01). The weak correlation in CH_4 is probably due to that CH_4 has a much

larger vertical gradient than the CO_2 between the troposphere and the stratosphere (Sepúlveda et al. 2014). Therefore, vertical transport in the upper troposphere and lower stratosphere (UTLS) and horizontal transport in the stratosphere both make strong impacts on CH_4 column. Nevertheless, the CH_4 enhancement on 16 May was observed both near the surface and in the column.

To better understand the enhancement of CO_2 and CH_4 at QOMS on 16 May, we use the FLEXPART_v10.4 backward simulations (Pisso et al., 2019) to show where the sources of the airmass are coming from during this campaign. The main settings of the FLEXPART model are listed in Table 3. Figure 6 shows the backward sensitivities on 7, 16 and 21 May 2022. Compared to 7 and 21 May, there is a significant airmass at QOMS on 16 May coming from North India, with higher gas concentrations. It is inferred that the enhancement of the measurements on 16 May 2022 is mainly due to the atmospheric transport.

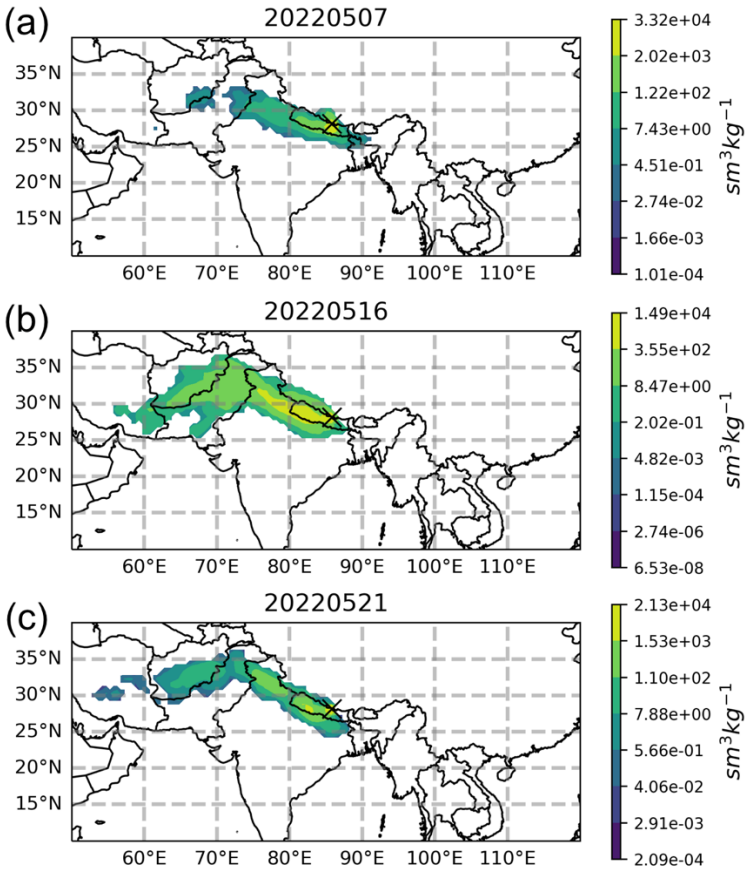

Figure 6. The spatial distribution of air backward sensitivities at QOMS between 04:00-05:00 (UTC) on 7, 16, 21 May 2022. The QOMS site is marked with a cross symbol.

Table 3. The key settings of FLEXPART model backward run.

Parameter	Settings
Tracer	Air
Release location	±0.05° around QOMS
Release height	0-1000 m a.g.l.
Release time	04:00-05:00 (UTC)
Number of backward running days	3 days
Number of releasing particles	20000
Meteorological data	NCEP CFSv2 with 0.5° × 0.5° horizontal resolution and 64 vertical levels

4.2 Ground-based FTIR against TROPOMI XCO measurements

In this section, we compare the ground-based EM27/SUN FTIR measurements (GB) to the TROPOMI satellite XCO measurements (SAT) at QOMS. We use the mean of GB measurements within ±2 hours of each satellite overpass time (approximately from 12:30 to 17:30 LT), and select all the satellite measurements within a certain distance around QOMS. For each SAT-GB data pair, we apply the SAT *a priori* profile (TM5 model) as the common prior to reducing the uncertainty from different *a priori* profiles (Rodgers and Connor 2003). In addition, to get rid of the discrepancy caused by different surface altitudes of the FTIR and satellite measurements, the FTIR retrieved XCO is scaled to the same vertical range of each satellite measurement (Langerock et al. 2015). Figures 7b and 7c show the mean and std of the differences between co-located TROPOMI satellite and ground-based FTIR XCO measurements (SAT-GB) between 5 and 24 May, varying with the co-located distance criterion ranging from 10 to 105 km. The mean difference varies between -3.9 and -6.3 ppb. The mean difference enlarges with increasing distance between FTIR and TROPOMI measurements, while the std reaches the minimum (5.36 ppb) at the distance of 25 km. To ensure enough data pairs to get a robust comparison, we set the co-located distance to 25 km, resulting in 17 days with co-located FTIR and satellite measurements.

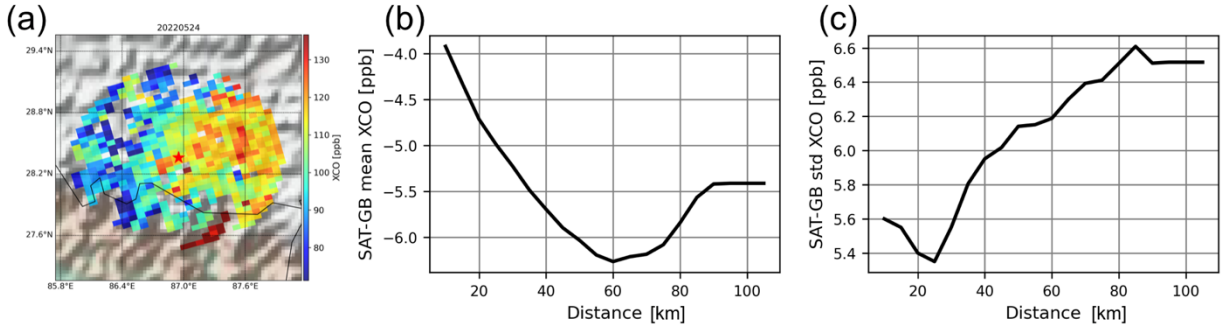

Figure 7. The TROPOMI XCO measurements within 100 km around the QOMS (red star) on 24 May 2022 (a). The mean (b) and std (c) of the differences between co-located TROPOMI satellite

and ground-based EM27/SUN XCO measurements (SAT-GB) between 5 and 24 May varying with the co-located distance criterion.

The time series and scatter plot of the co-located FTIR and TROPOMI satellite XCO measurements at QOMS are shown in Figure 8. A good correlation between FTIR and TROPOMI XCO measurements is observed, with the R value of 0.81 (p_value<0.001). The difference between FTIR and TROPOMI XCO measurements is -5.06±5.36 ppb (-4.7±5.1%), which is within the S5P mission requirements with a systematic error of 15% and random error of 10%. The relative bias at QOMS is also comparable with other places around the world (Sha et al. 2021; Martínez-Alonso et al. 2022). The EM27/SUN measurements at QOMS thus indicate that the TROPOMI XCO data has a good performance in this region.

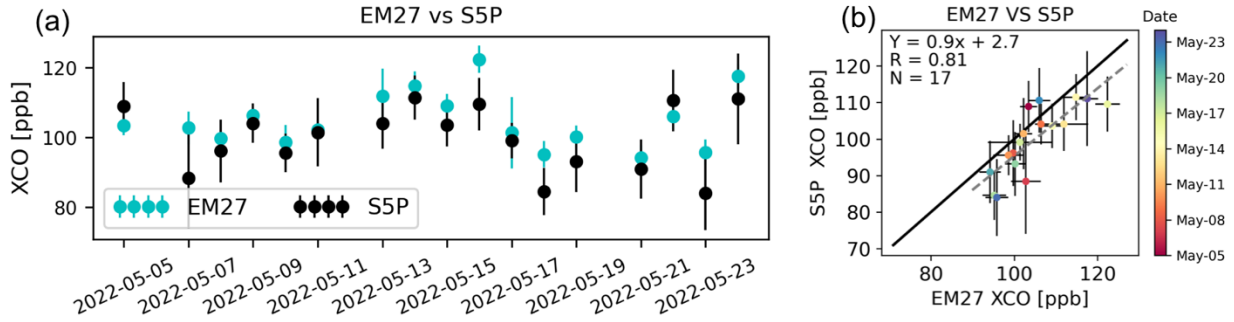

Figure 8. The co-located TROPOMI/S5P and EM27/SUN XCO measurements between 5 and 24 May 2022 (a). The errorbar of the satellite measurement is the std of all measurements within 25 km around the site, and the errorbar of the FTIR measurement is the std of all measurements within ±2 hours within the satellite overpass time. The scatter plot of the TROPOMI/S5P and EM27/SUN XCO co-located measurements (b). The dashed line is the linear regression, R is the Pearson correlation coefficient, and N is the number of the co-located measurements. The dot is colored by the measurement date.

The high and low XCO values at QOMS are observed simultaneously from the ground-based FTIR and TROPOMI satellite measurements. Thanks to the good coverage of the TROPOMI satellite measurements, it is applied to show the spatial distributions of XCO around QOMS in a larger domain. Figure 9 shows the TROPOMI XCO measurements on 16, 22, and 24 May with relatively high XCO values, and on 18, 21, and 23 May, with relatively low XCO values around QOMS. The wind speed and wind direction are derived from the ERA5 reanalysis pressure-level data at 500 hPa (~ 5 km a.s.l.). We find that XCO at the south side of Mt. Qomolangma is much larger than that at the side edge, because of high anthropogenic emissions in Nepal and India

(Crippa et al. 2018). The relatively high XCO values at QOMS on 16, 22, and 24 May correspond to south winds, which bring the airmass with high CO mole fraction to QOMS. On 18 and 21 May, the wind direction was from the west to the east along the southern edge of the Himalayas mountains and did not bring airmass to QOMS so low XCO values are observed in all regions of the southern Tibetan Plateau. On 23 May, relatively high XCO values are observed at approximately 200 km west or east of QOMS, but low XCO values are observed at QOMS. Based on the TROPOMI satellite measurements and the wind data, we conclude that the day-to-day variation of XCO observed at QOMS is largely influenced by atmospheric transport, and the airmass transported from southern Asia can enhance the CO mole fractions over the Tibetan Plateau.

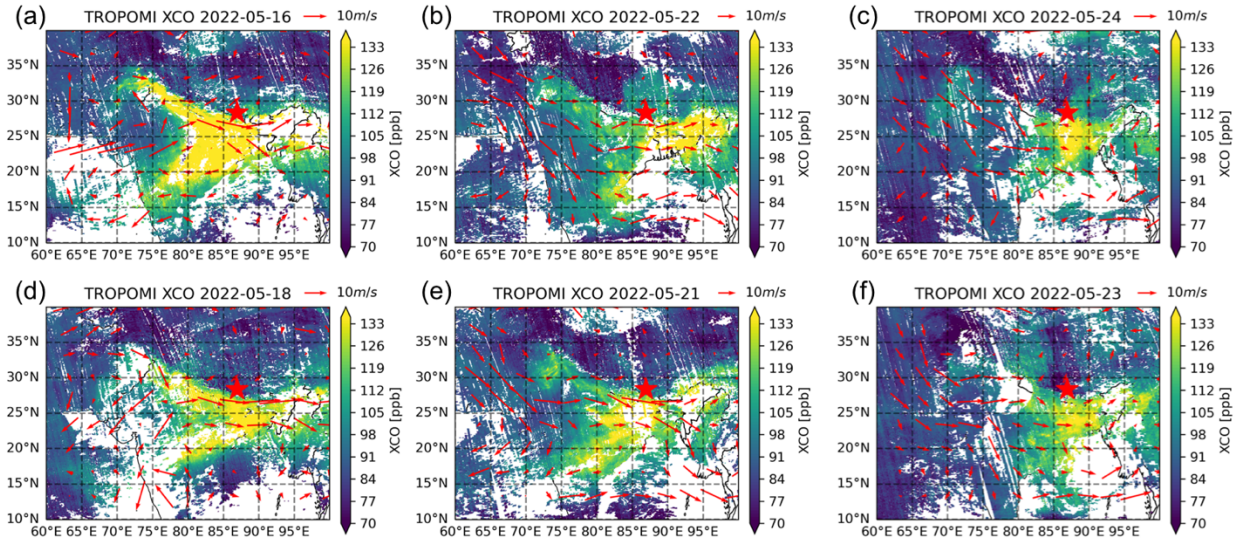

Figure 9. The XCO observed by the TROPOMI/S5P satellite on 16 (a), 22 (b), and 25 (c) May 2022, with relatively high XCO values at QOMS (the red star), and on 18 (d), 21 (e), and 23 (f) May 2022, with relatively low XCO values at QOMS. The wind direction and wind speed are derived from the ERA5 reanalysis data at 500 hPa (~ 5 km a.s.l.).

4.3 Ground-based FTIR against OCO-2 XCO_2 measurements

Unlike the TROPOMI XCO measurements, very limited OCO-2 XCO_2 measurements are available due to its narrow swath. During this campaign, we only had two days, when the OCO-2 satellite provided valid measurements (qflag = 0) around QOMS (Figure 10). The distances between the OCO-2 measurements and the FTIR site are about 480 km and 250 km on 8 and 24 May, respectively. Note that the observation mode of OCO-2 is land glint on 8 May and land nadir on 24 May. As the OCO-2 and EM27/SUN both use GEOS-FPIT model simulations as the *a priori*

profiles, no prior substitution correction is needed (Zhou et al. 2016). For each FTIR-satellite data pair, we correct the FTIR measurement to the same altitude of the satellite footprint. As we do not have the FTIR measurement around the OCO-2 overpass time (~15:30 CST), we use the mean of the FTIR measurements in the latest 1 hour.

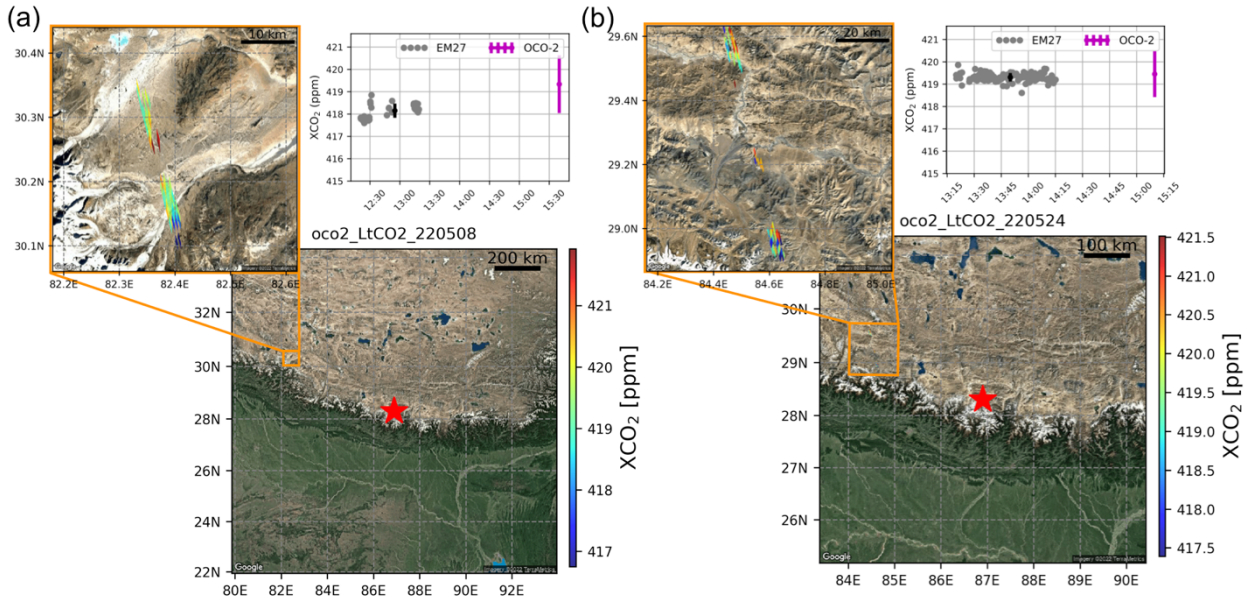

Figure 10. The XCO_2 observed by the OCO-2 satellite with glint mode on 8 May (a) and with nadir mode on 24 May (b) around QOMS (the red star on the satellite image from © Google Maps). For each day, the time series of the EM27/SUN XCO_2 individual measurements in the latest 1 hour are shown together with the mean and std of EM27/SUN measurements (black) and all co-located OCO-2 measurments (magenta) in the top right panels.

The mean and std of the differences between EM27/SUN and OCO-2 XCO_2 measurements (SAT-GB) are 1.21±1.29 ppm and 0.21±0.98 ppm on 8 and 24 May, respectively. The bias of OCO-2 XCO_2 measurements at QOMS is in the same order of magnitude as the bias found at global TCCON sites (Wunch et al. 2017). The repo rted uncertainty of the OCO-2 XCO_2 nadir measurements on 24 May is 0.65 ppm, which is slightly lower than the std of 0.98 ppm. However, the reported uncertainty of the OCO-2 XCO_2 glint measurements on 8 May is 0.57 ppm, which is much smaller than the std of 1.29 ppm.

As the footprint of OCO-2 is a bit far away from the QOMS site, we use the Copernicus Atmosphere Monitoring Service (CAMS) model simulations (Agustí-Panareda et al., 2023) in May 2020 to estimate the spatial variability of XCO_2 between the QOMS and OCO-2 footprints in this study. The mean and std of the differences in CAMS XCO_2 between the QOMS and OCO-

2 footprint around 29.2°N, 84.5°E (~250 km) are 0.02 ppm and 0.27 ppm, respectively. The mean and std of the differences in CAMS XCO_2 between the QOMS and OCO-2 footprint around 30.2°N, 82.4°E (~480 km) are 0.10 ppm and 0.34 ppm, respectively. According to the CAMS model simulations, the XCO_2 spatial variability in this region is relatively small.

The OCO-2 measurements on these two days are both concentrated in a small region without intense human activity. It is assumed that the XCO_2 is stable in such a region. Figure 11 shows the bias of OCO-2 glint measurements (SAT-GB) varying with surface altitudes and retrieved surface albedos in the O_2-A band on 8 May 2022. It is found that the bias of OCO-2 land glint measurements is strongly related to the retrieved surface albedos (R=0.54) and footprint surface altitudes (R=0.48). Further correction of OCO-2 glint measurements in this region using the O_2-A band surface albedo/surface altitude is recommended, but more data are required. Regarding the OCO-2 land nadir measurements on 24 May, we do not find significant correlations between the bias and altitudes (R=-0.26) or surface albedos (R=0.17). Instead, the biases are randomly distributed.

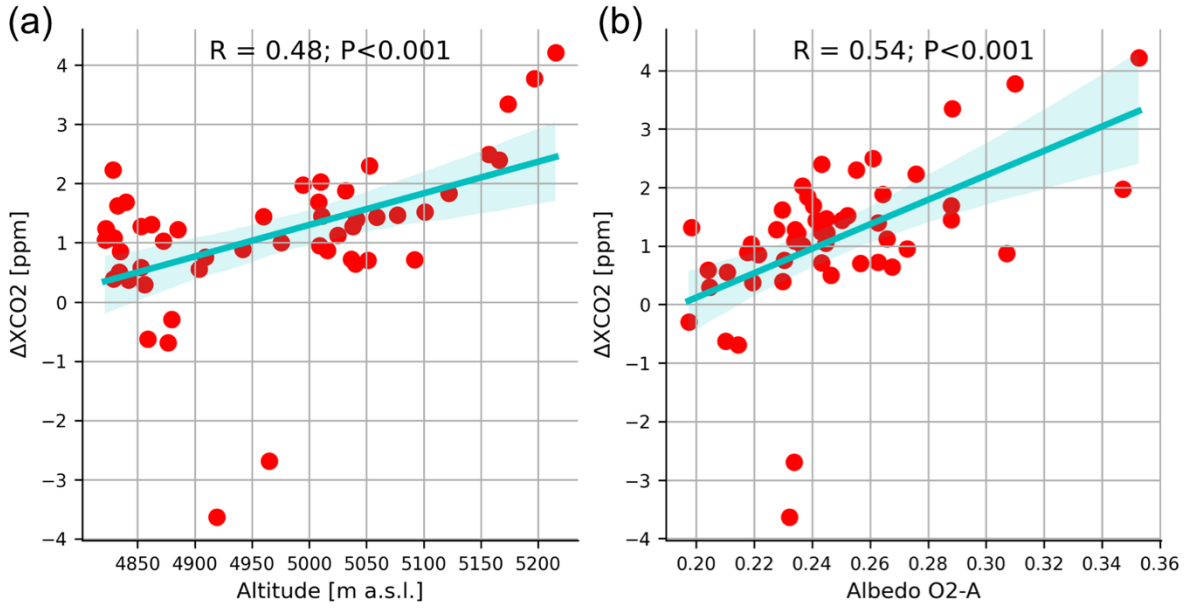

Figure 11. The bias of XCO_2 observed by OCO-2 land glint measurements (ΔXCO_2 = SAT-GB) on 8 May 2022 varying with surface altitude (a) and surface albedo in O_2-A band (b).

5 Conclusions

The QTP serves as a huge carbon storage but is also sensitive to climate change. Currently, there is still a large uncertainty about the terrestrial ecosystem carbon sink in the QTP. Due to the

tough environment, GHG measurements are scarce. In May 2022, an integrated greenhouse gases measurement campaign was carried out at QOMS within the framework of the Second Tibetan Plateau Scientific Expedition Program. In this study, we present the experiments about the *in situ* measurements near the surface and the ground-based EM27/SUN FTIR column measurements. The following results are presented and discussed:

1) The *in situ* measurements near the surface at QOMS between 13 and 24 May 2022 show that the CO_2 and CH_4 mole fractions are 424.2±2.1 ppm and 1985.2±19.7 ppb, respectively. In addition, a good correlation (R=0.82) between the surface CO_2 and CH_4 mole fractions is observed.
2) The ground-based FTIR measurements at QOMS between 5 and 24 May show that the mean XCO_2, XCH_4, XCO, and XN_2O are 418.4±0.6 ppm, 1888.3±8.0 ppb, 106.2±8.3 ppb, and 321.6±3.2 ppb, respectively. The mean of XCO_2 at QOMS is about 0.5-3.5 ppm lower than six TCCON sites in the mid-latitude northern hemisphere during the same time period. The GHG measurements at QOMS seriously differ from the GEOS-PFIT model simulations, indicating the large uncertainty of the model simulations in this region.
3) The ground-based FTIR measurements at QOMS are compared to TROPOMI XCO satellite observations. The difference between FTIR and TROPOMI XCO measurements is -5.06±5.36 ppb (-4.7±5.1%), which is within the S5P mission requirements. A good correlation between FTIR and TROPOMI XCO measurements is also found, with an R of 0.81. Utilizing the good spatial coverage of TROPOMI satellite measurements together with the wind data, we find that the day-to-day variation of XCO observed at QOMS is largely affected by atmospheric transport. It is important to carry out long-term measurements to calculate the cross-regional transport in this region quantitatively.
4) The ground-based FTIR measurements at QOMS are also compared to OCO-2 XCO_2 observations. There were only two days with OCO-2 measurements within 500 km around QOMS (land glint mode on 8 May 2022 and land nadir mode on 24 May 2022). The mean differences between FTIR and OCO-2 XCO_2 measurements are 1.21±1.29 ppm and 0.21±0.98 ppm on 8 and 24 May, respectively. It is found that the bias of OCO-2 glint measurements on 8 May is relatively large, and it is statistically related to the retrieved surface albedos and surface altitudes. The quality of the OCO-2 XCO_2 land glint

measurements in this region should be further assessed when more ground-based measurements become available.

Appendix I

The uncertainties of the EM27/SUN CO_2, CH_4, CO and N_2O measurements at QOMS are estimated by perturbing the inputs using the GGG2020 code. In this study, we include contributions from instrumental effects (ILS), observation geometry (pointing offset), temperature profile, spectroscopy (line intensity), a priori dependence, and measurement noise (Table A1).

Table A1. List of sources, values used for the uncertainty analysis, and CO_2, CH_4, CO and N_2O column retrieval uncertainties for all measurements at QOMS site using the GGG2020 code. (ME: modulation efficiency amplitude; SNR: signal-to-noise ratio). The third column provides the partitioning of the error values between random (ran) and systematic (sys) contributions. Note that an uncertainty less than 0.01% is indicated as '-'.

Error source	Uncertainty value	sys/ran contribution [%]	CO_2 column uncertainty (sys/ran) [%]	CH_4 column uncertainty (sys/ran) [%]	CO column uncertainty (sys/ran) [%]	N_2O column uncertainty (sys/ran) [%]
Prior	2%	50/50	0.01/0.01	0.02/0.02	0.04/0.04	0.08/0.08
ILS (ME and phase error)	1% and 0.01rad	50/50	0.1/0.1	0.1/0.1	0.1/0.1	0.1/0.1
Pointing offset	0.1°	10/90	-/0.1	-/0.1	-/0.1	-/0.2
Temperature profile	2 K	50/50	0.03/0.03	0.15/0.15	0.80/0.80	0.07/0.07
Spectroscopy	2%	100/0	2.0/-	2.0/-	2.0/-	2.0/-
Measurement noise	1/SNR	0/100	-/0.1	-/0.1	-/0.3	-/1.2
Total			2.0/0.2	2.0/0.2	2.0/0.9	2.0/1.2

Data availability

The TCCON data were obtained from the TCCON Data Archive hosted by CaltechDATA at https://tccondata.org. The TROPOMI satellite data are available at https://dataspace.copernicus.eu/ (registration request). OCO-2 satellite data are available at https://ocov2.jpl.nasa.gov/science/oco-2-data-center/ (registration request). The ground-based FTIR measurements at QOMS are available upon request. The CAMS model simulations are publicly available at https://ads.atmosphere.copernicus.eu/datasets/cams-global-ghg-reanalysis-egg4?tab=overview.

Competing interests

The authors declare that they have no conflict of interest.

Acknowledge

This study is supported by Second Tibetan Plateau Scientific Expedition Program (2022QZKK0101), the National Natural Science Foundation of China (42205140), and the Youth Innovation Promotion Association, CAS (2023077). The authors would like to thank all stuffs at QOMS for supporting the GHG measurement campaign. The authors want to thank TCCON community, ESA, and NASA for providing the TCCON, TROPOMI and OCO-2 data.

Author contributions

MZ, YW, and MZ design the study. MZ wrote the manuscript with inputs from YW and MZ. XT and JD serve as the project leaders of the campaign. JB set up the EM27/SUN instrument. YM, WM, and ZX provided local support to collect the data. All authors have read and commented the manuscript.

Reference:

Agustí-Panareda, A and Coauthors, 2023: Technical note: The CAMS greenhouse gas reanalysis from 2003 to 2020, Atmos. Chem. Phys., 23, 3829–3859.

Borsdorff, T., and Coauthors, 2019: Improving the TROPOMI CO data product: update of the spectroscopic database and destriping of single orbits. *Atmospheric Meas. Tech.*, **12**, 5443–5455.

Crippa, M., and Coauthors, 2018: Gridded emissions of air pollutants for the period 1970–2012 within EDGAR v4. 3.2. *Earth Syst Sci Data*, **10**, 1987–2013.

Ding, J., and Coauthors, 2016: The permafrost carbon inventory on the Tibetan Plateau: a new evaluation using deep sediment cores. *Glob. Change Biol.*, **22**, 2688–2701, https://doi.org/10.1111/gcb.13257.

García, O. E., Schneider, M., Herkommer, B., Gross, J., Hase, F., Blumenstock, T., & Sepúlveda, E. (2022). TCCON data from Izana, Release GGG2020.R1. https://doi.org/10.14291/tccon.ggg2020.izana01.R1

Ge, F., F. Sielmann, X. Zhu, K. Fraedrich, X. Zhi, T. Peng, and L. Wang, 2017: The link between Tibetan Plateau monsoon and Indian summer precipitation: a linear diagnostic perspective. *Clim. Dyn.*, **49**, 4201–4215, https://doi.org/10.1007/s00382-017-3585-1.

Guo, M., and Coauthors, 2020: Comparison of atmospheric CO2, CH4, and CO at two stations in the Tibetan Plateau of China. *Earth Space Sci.*, **7**, e2019EA001051.

Hase, F., B. Herkommer, J. Groß, T. Blumenstock, M. ä. Kiel, and S. Dohe, 2023: TCCON data from Karlsruhe (DE), Release GGG2020.R1. https://doi.org/10.14291/tccon.ggg2020.karlsruhe01.R1.

Ji, D., and Coauthors, 2020: Deriving temporal and vertical distributions of methane in Xianghe Using ground-based Fourier transform infrared and gas-analyzer measurements. *Adv. Atmospheric Sci.*, **37**, 597–607.

Jia, L., and Coauthors, 2021: Carbon storage of the forest and its spatial pattern in Tibet, China. *J. Mt. Sci.*, **18**, 1748–1761.

Jiang, F., and Coauthors, 2016: A comprehensive estimate of recent carbon sinks in China using both top-down and bottom-up approaches. *Sci. Rep.*, **6**, 22130.

Keppel-Aleks, G., and Coauthors, 2012: The imprint of surface fluxes and transport on variations in total column carbon dioxide. *Biogeosciences*, **9**, 875–891.

Kiel, M., C. W. O'Dell, B. Fisher, A. Eldering, R. Nassar, C. G. MacDonald, and P. O. Wennberg, 2019: How bias correction goes wrong: measurement of X< sub> CO< sub> 2</sub></sub> affected by erroneous surface pressure estimates. *Atmospheric Meas. Tech.*, **12**, 2241–2259.

Landgraf, J., and Coauthors, 2016: Carbon monoxide total column retrievals from TROPOMI shortwave infrared measurements. *Atmospheric Meas. Tech.*, **9**, 4955–4975.

Langerock, B., M. De Mazière, F. Hendrick, C. Vigouroux, F. Desmet, B. Dils, and S. Niemeijer, 2015: Description of algorithms for co-locating and comparing gridded model data with remote-sensing observations. *Geosci. Model Dev.*, **8**, 911–921.

Laughner, J. L., and Coauthors, 2023: A new algorithm to generate a priori trace gas profiles for the GGG2020 retrieval algorithm. *Atmospheric Meas. Tech.*, **16**, 1121–1146.

Liu, S., and Coauthors, 2021: Changes of atmospheric CO2 in the Tibetan Plateau from 1994 to 2019. *J. Geophys. Res. Atmospheres*, **126**, e2021JD035299.

Lorente, A., and Coauthors, 2021: Methane retrieved from TROPOMI: improvement of the data product and validation of the first 2 years of measurements. *Atmospheric Meas. Tech.*, **14**, 665–684.

Ma, Y., and Coauthors, 2023: QOMS: A Comprehensive Observation Station for Climate Change Research on the Top of Earth. *Bull. Am. Meteorol. Soc.*, **104**, E563–E584, https://doi.org/10.1175/BAMS-D-22-0084.1.

Martínez-Alonso, S., M. N. Deeter, B. C. Baier, K. McKain, H. Worden, T. Borsdorff, C. Sweeney, and I. Aben, 2022: Evaluation of MOPITT and TROPOMI carbon monoxide retrievals using AirCore in situ vertical profiles. *Atmospheric Meas. Tech.*, **15**, 4751–4765.

O'dell, C. W., and Coauthors, 2018: Improved retrievals of carbon dioxide from Orbiting Carbon Observatory-2 with the version 8 ACOS algorithm. *Atmospheric Meas. Tech.*, **11**, 6539–6576.

520 Piao, S., Y. He, X. Wang, and F. Chen, 2022: Estimation of China's terrestrial ecosystem carbon
521 sink: Methods, progress and prospects. *Sci. China Earth Sci.*, **65**, 641–651.

522 Pisso, I., and Coauthors, 2019: The Lagrangian particle dispersion model FLEXPART version
523 10.4, Geosci. Model Dev., 12, 4955–4997.

524 Rodgers, C. D., and B. J. Connor, 2003: Intercomparison of remote sounding instruments. *J.*
525 *Geophys. Res. Atmospheres*, **108**.

526 Rui, Y., and Coauthors, 2011: Warming and grazing affect soil labile carbon and nitrogen pools
527 differently in an alpine meadow of the Qinghai–Tibet Plateau in China. *J. Soils*
528 *Sediments*, **11**, 903–914, https://doi.org/10.1007/s11368-011-0388-6.

529 Sepúlveda, E., and Coauthors, 2014: Tropospheric CH 4 signals as observed by NDACC FTIR at
530 globally distributed sites and comparison to GAW surface in situ measurements.
531 *Atmospheric Meas. Tech.*, **7**, 2337–2360.

532 Sha, M. K., and Coauthors, 2021: Validation of methane and carbon monoxide from Sentinel-5
533 Precursor using TCCON and NDACC-IRWG stations. *Atmospheric Meas. Tech.*, **14**,
534 6249–6304.

535 Tada, R., H. Zheng, and P. D. Clift, 2016: Evolution and variability of the Asian monsoon and its
536 potential linkage with uplift of the Himalaya and Tibetan Plateau. *Prog. Earth Planet.*
537 *Sci.*, **3**, 4, https://doi.org/10.1186/s40645-016-0080-y.

538 Té, Y., P. Jeseck, and C. Janssen, 2022: TCCON data from Paris (FR), Release GGG2020.R0.
539 https://doi.org/10.14291/tccon.ggg2020.paris01.R0.

540 Wang, R., and Coauthors, 2021: Monthly Patterns of Ammonia Over the Contiguous United
541 States at 2-km Resolution. *Geophys. Res. Lett.*, **48**,
542 https://doi.org/10.1029/2020GL090579.

543 Wang, T., D. Yang, Y. Yang, S. Piao, X. Li, G. Cheng, and B. Fu, 2020: Permafrost thawing
544 puts the frozen carbon at risk over the Tibetan Plateau. *Sci. Adv.*, **6**, eaaz3513,
545 https://doi.org/10.1126/sciadv.aaz3513.

546 Wang, Y., Z. Ding, and Y. Ma, 2022: Data processing uncertainties may lead to an
547 overestimation of the land carbon sink of the Tibetan Plateau. *Proc. Natl. Acad. Sci.*, **119**,
548 e2202343119.

549 Wang, Z., and Coauthors, 2014: Retrieval of tropospheric column-averaged CH 4 mole fraction
550 by solar absorption FTIR-spectrometry using N 2 O as a proxy. *Atmospheric Meas.*
551 *Tech.*, **7**, 3295–3305.

552 Warneke, T., C. Petri, J. Notholt, and M. Buschmann, 2022: TCCON data from Orléans (FR),
553 Release GGG2020.R0. https://doi.org/10.14291/tccon.ggg2020.orleans01.R0.

Wennberg, P. O., C. M. Roehl, D. Wunch, J.-F. Blavier, G. C. Toon, N. T. Allen, R. Treffers, and J. Laughner, 2022a: TCCON data from Caltech (US), Release GGG2020.R0. https://doi.org/10.14291/tccon.ggg2020.pasadena01.R0.

Wennberg, P. O., D. Wunch, C. M. Roehl, J.-F. Blavier, G. C. Toon, and N. T. Allen, 2022b: TCCON data from Lamont (US), Release GGG2020.R0. https://doi.org/10.14291/tccon.ggg2020.lamont01.R0.

Wu, J., and Coauthors, 2021: Disentangling climatic and anthropogenic contributions to nonlinear dynamics of alpine grassland productivity on the Qinghai-Tibetan Plateau. *J. Environ. Manage.*, **281**, 111875, https://doi.org/10.1016/j.jenvman.2020.111875.

Wunch, D., and Coauthors, 2011: The total carbon column observing network. *Philos. Trans. R. Soc. Math. Phys. Eng. Sci.*, **369**, 2087–2112.

Wunch, D., and Coauthors, 2017: Comparisons of the orbiting carbon observatory-2 (OCO-2) X CO 2 measurements with TCCON. *Atmospheric Meas. Tech.*, **10**, 2209–2238.

Yang, and Coauthors, 2020: New ground-based Fourier-transform near-infrared solar absorption measurements of \chemXCO_2, \chemXCH_4 and \hack\breakXCO at Xianghe, China. *Earth Syst. Sci. Data*, **12**, 1679–1696, https://doi.org/10.5194/essd-12-1679-2020.

Yang, Z., G. C. Toon, J. S. Margolis, and P. O. Wennberg, 2002: Atmospheric CO2 retrieved from ground-based near IR solar spectra. *Geophys. Res. Lett.*, **29**, 53–1.

Zhang, G., Z. Nan, L. Zhao, Y. Liang, and G. Cheng, 2021: Qinghai-Tibet Plateau wetting reduces permafrost thermal responses to climate warming. *Earth Planet. Sci. Lett.*, **562**, 116858, https://doi.org/10.1016/j.epsl.2021.116858.

Zhang, Y., and Coauthors, 2015: Effects of grazing and climate warming on plant diversity, productivity and living state in the alpine rangelands and cultivated grasslands of the Qinghai-Tibetan Plateau. *Rangel. J.*, **37**, 57–65.

Zhou, M., and Coauthors, 2016: Validation of TANSO-FTS/GOSAT XCO 2 and XCH 4 glint mode retrievals using TCCON data from near-ocean sites. *Atmospheric Meas. Tech.*, **9**, 1415–1430.

Zhou, M., and Coauthors, 2018: Atmospheric CO and \chemCH_4 time series and seasonal variations on Reunion Island from ground-based in situ and FTIR (NDACC and TCCON) measurements. *Atmospheric Chem. Phys.*, **18**, 13881–13901, https://doi.org/10.5194/acp-18-13881-2018.

Zhou, M., P. Wang, N. Kumps, C. Hermans, and W. Nan, 2022: TCCON data from Xianghe, China, Release GGG2020.R0. https://doi.org/10.14291/tccon.ggg2020.xianghe01.R0.

Zhou, M., and Coauthors, 2023: Ground-Based Atmospheric CO2, CH4, and CO Column Measurements at Golmud in the Qinghai-Tibetan Plateau and Comparisons with

589 TROPOMI/S5P Satellite Observations. *Adv. ATMOSPHERIC Sci.*, **40**, 223–234,
590 https://doi.org/10.1007/s00376-022-2116-0.

591